

Impact of the Low-level Controller on String Stability of Adaptive Cruise Control System

Hao Zhou¹, Anye Zhou¹, Tienan Li², Danjue Chen², Srinivas Peeta¹, Jorge Laval^{*1}

Abstract—Current factory adaptive cruise control (ACC) systems consist of an upper-level planner that computes the optimal trajectory of the vehicle and a low-level controller in charge of executing it. The literature on the string stability (SS) of ACC systems is mostly concerned with the upper-level planner. In this paper, we show that the low-level controller can have a significant impact on SS. We find that i) a fast controller improves the SS, ii) a slow controller can result from either insufficient control gains or from an undershooting gas/brake system or both, and iii) although the integral gain is helpful for effective control, the integral windup can cause overshooting, and in turn undermines the SS of the ACC. Accordingly, we suggest tuning up the proportional/feedforward gain and ensuring the gas/brake is not to undershoot. Anti-windup design is also needed to improve SS. The results of this paper are validated both numerically and empirically on commercial cars.

Index Terms—string stability, low-level controller, ACC

I. INTRODUCTION

With the development of vehicle automation, adaptive cruise control (ACC) systems are now widely available on vehicles around the world. To be beneficial in terms of traffic efficiency, ACC systems are expected to achieve string stability (SS) to ensure that small perturbations do not amplify along a platoon of vehicles [1], [2], i.g., speed fluctuations should be dampened, rather than amplified by the follower [3], [4]. A commercial ACC system is typically comprised of an upper-level planner and a low-level controller. The planner uses sensor data to estimate the kinematic information of preceding vehicles (e.g., spacing, speed) and output a desired speed/acceleration. Then the low-level controller incorporates the planning outputs and tries to actually move the vehicle towards the desired speed/acceleration target.

In recent years, the SS of ACC systems has drawn increasing attention from the traffic flow community, in the context of fast developing self-driving technologies and their potential impact on traffic flow efficiency. Since the ACC modules on commercial car models are "black boxes", researchers can only collect some empirical driving data of the ACC systems, and retrofit them with some controllers or car-following (CF) models to investigate the SS by simulations [5], [6].

On the other hand, the SS of ACC systems has been studied since the turn of the millennium in the control area [7]–[9]. There are a plethora of studies working towards the design of string stable ACC or cooperative adaptive cruise control (CACC) systems. Most of studies focus on deriving the theoretical SS condition of a simplified upper-level planner, and some studies validate SS performance using real-car experiments [10], [11]. However, the impact of low-level controllers has yet been neglected. This phenomenon can be explained by the fact that most testing cars in SS experiments are retrofitted, using different hardwares compared to commercial vehicles and operating on customized platform such as the robot operating system, rather than the commercial ACC systems.

Meanwhile, existing study also points out most commercial ACC systems are string-unstable [12]. In particular, [9] conjectures that string-unstable ACCs are likely due to the vehicle actuators driven by low-level controller cannot perfectly follow the upper-level planner. However, an explicit analysis of the impact is missing. In addition, [11], [13] recognize the existence and potential impact of low-level controllers but still treated them as a black-boxes. So far the impact of low-level controller has not been studied in detail, and pertinent experiments on real cars are still missing.

Furthermore, for commercial ACC vehicles, although empirical ACC data has been collected and used for retrofitting, to the best of our knowledge, no commercial ACC algorithms have been investigated and evaluated. To fill in voids of evaluating low-level controller and investigating commercial ACC algorithms, this paper dives into the open-source commercial ACC algorithms in Openpilot [14], a self-driving software published by Comma.ai, one of the leading self-driving tech companies with more than 40 million miles of drives [14]. The after-market ACC device of Comma.ai is called Comma Two, which connects and overwrites the stock ACC modules on commercial cars with its own self-driving software Openpilot. The Openpilot software is not only open-source, but also allows users to customize their own ACC algorithm and test it on real cars, which is aligned with the objective of this study, and enables us to highlight the differences between commercial ACC system in the real world and the simplified controller/CF models in the literature. Correspondingly, with an emphasis on the impact of the low-level controller, this study not only analytically analyzes the impact mechanisms of low-level controller, but also leverages the software (Openpilot) and hardware (Comma Two) from Comma.ai to validate our findings using simulations and real-car tests.

The remainder of the paper is organized as follows: section

*Coresponding author

This work is supported by the NSF Grant ... and ...

¹H. Zhou, A. Zhou, J. Laval, and S. Peeta are with the School of Civil and Environmental Engineering, Georgia Institute of Technology, Atlanta, GA 30332, USA (e-mail: zhouhao, azhou46, peeta@gatech.edu, jorge.laval@ce.gatech.edu).

²T. Li and D. Chen are with the Department of Civil and Environmental Engineering, University of Massachusetts, Lowell, MA 01854, USA (e-mail: tienan_li@student.uml.edu, danjue_chen@uml.edu)

II introduces the factory ACC algorithms used in Openpilot; section III presents the detailed mechanism of the impact of the low-level controller on SS; section IV showcases the simulation results; section V validates the major findings using real drives on commercial cars running Openpilot; section VI concludes the paper and discusses future directions.

II. BACKGROUND

A. Pipeline for the longitudinal control in Openpilot

Fig. 1 shows the pipeline of the longitudinal control of self-driving cars in Openpilot. The longitudinal control starts with a planner running at 20hz (equal to the radar sampling rate) which outputs a target speed, v_{target} , or target acceleration, a_{target} , based on certain type of (car-following) CF models. The target value is then passed on to the low-level controller. Notice that the low-level controller runs at the 100 hz, which is required by the gas/brake system of a modern car. Hence every planning period would consist of 5 consecutive control steps. For the low-level controller, the logic is as follows: i) the speed or acceleration setpoint, v_{pid} and a_{pid} , for each of the 5 control steps is first computed based on v_{target} or a_{target} ; ii) then a proportional-integral (PI) or proportional-integral-feedforward (PIF) controller is designed to achieve v_{pid} or a_{pid} by outputting the *control* input; iii) the control input is then fed to a processor that maps it to the actuator command, which is a gas or brake percent gb for the car. We refer to this process as the *compute_gb* function. If we view the *control* variable as the desired acceleration, then the *compute_gb* function is a mapping from an acceleration to a gas/brake percentage. Conversely, we can call the mapping from gb to the true accelerations the *gb2accel* function which largely depends on the engine and braking performances of a car. The gas/brake percentage is then applied on the ego vehicle to obtain the true acceleration a_{ego} , speed v_{ego} , and position x_{ego} .

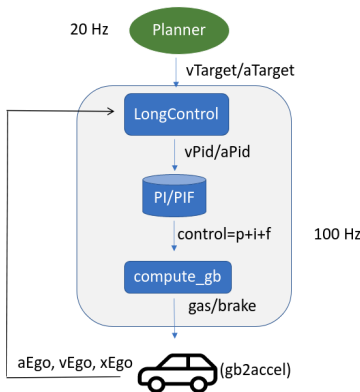


Fig. 1: Pipeline for longitudinal control.

B. The Upper-level planner

1) *The linear planner*: As mentioned previously, the planner can be a linear/non-linear controller, or a CF model in

traffic domain. Here we start with a regular linear-controller type planner with constant time headway policy (CTH), which is common on factory ACC systems. Given a desired time headway H_t , and the jam spacing s_j , the desired spacing s_{des} between the ego vehicle and the lead vehicle is calculated as:

$$s_{des} = s_j + H_t \cdot v_{lead} \quad (1)$$

Then the planner outputs a target speed v_{target} (2) to reduce the error between the true spacing s_{lead} and the desired spacing s_{des} by a rate k_v . Note that in practice, k_v is a function of v_{ego} , rather than a constant applied in existing literature [5], [15].

$$v_{target} = (s_{lead} - s_{des}) \cdot k_v + v_{lead} \quad (2)$$

The actual v_{target} will be further constrained by acceleration limits from multiple sources such as comfortableness, the vehicle dynamics, maximum speed difference from the leader, and the impact of curves.

2) *MPC planner*: For a regular commercial vehicle, a professional solver (for example Acado [16]) is needed for an MPC planner to compile and run in real time. Consequently, the MPC controller follows a predefined optimization framework required by the solver. The formulation of the optimization objective and the reference trajectory are two key components for an MPC problem, while how to solve it is out of scope for this paper. Now we will introduce these two key components.

In Openpilot the objective function $C(\hat{t})$ for the longitudinal MPC at the planning time \hat{t} is defined as a weighted sum of four sub-costs, with respect to the time to collision, spacing, acceleration and jerk values:

$$C(\hat{t}) = \sum_{\hat{t} \leq k \leq \hat{t} + T_{mpc}} w_{ttc} C_{ttc}(k) + w_{dist} C_{dist}(k) + w_{accel} C_{accel}(k) + w_{jerk} C_{jerk}(k) \quad (3)$$

where T_{mpc} is the optimization horizon, the tunable weights applied here are $w_{ttc} = 5$, $w_{dist} = 0.1$, $w_{accel} = 10$, $w_{jerk} = 20$. The four sub-costs are defined as: $C_{ttc} = \exp\left\{\frac{s_{des} - s_{lead}}{(\sqrt{v_{ego} + 0.5} + 0.1)/0.3}\right\} - 1$, $C_{dist} = \frac{s_{des} - s_{lead}}{0.05v_{ego} + 0.5}$, $C_{accel} = a_{ego}(0.1v_{ego} + 1)$, and $C_{jerk} = j_{ego}(0.1v_{ego} + 1)$, where j_{ego} is the jerk of ego vehicle (i.e., derivative of acceleration), the desired spacing s_{des} for the MPC controller is defined as:

$$s_{des} = v_{ego} \cdot H_t - (v_{lead} - v_{ego}) \cdot H_t + \frac{v_{ego}^2 - v_{lead}^2}{2G} \quad (4)$$

where G is the gravity constant.

The reference trajectory for the MPC is the predicted lead vehicle trajectory estimated from a simple dynamics model in (5), which assumes a decaying acceleration of the lead vehicle with time parameter τ (1.5s) and dt_p (0.2s) denotes the step size along the MPC prediction horizon T_{mpc} (2.0s).

$$\begin{aligned} a_{lead} &\leftarrow a_{lead}(t_0) \exp(-\tau t^2/2) \\ x_{lead} &\leftarrow x_{lead} + v_{lead} \cdot dt_p \\ v_{lead} &\leftarrow v_{lead} + a_{lead} \cdot dt_p \\ \hat{t} &\leftarrow \hat{t} + dt_p \end{aligned} \quad (5)$$

By solving the MPC problem (6) at each time step \hat{t} , we can obtain the a_{target} for the low-level controller.

$$\begin{aligned} \min_{a_{target}} \quad & C(\hat{t}) \\ \text{s.t.} \quad & \text{Point-mass dynamics [17] for the ego car} \\ & \text{Predicted dynamics for the lead car in (5)} \\ & v_{target} \geq 0 \end{aligned} \quad (6)$$

It is worth noting that the MPC planner can also use the predicted ego vehicle trajectory as the reference, which is more straightforward but probably needs a vision-based machine learning model. Detailed discussion can be found in [18], [19].

Recall that a linear controller outputs a desired speed value v_{target} , which is all a low-level PI controller needs. However, it is a different case for a low-level PIF controller since it needs both v_{pid} and a_{pid} . Accordingly, except for the MPC solver, the MPC planner involves two more variables $v_{start}(\hat{t})$ and $a_{start}(\hat{t})$, which are updated using the following rule:

$$a_{start} \leftarrow a_{start} + d\hat{t}/dt_p(a_{target} - a_{start}) \quad (7)$$

$$v_{start} \leftarrow v_{start} + d\hat{t}(a_{target} + a_{start})/2 \quad (8)$$

where $d\hat{t}$ denotes the time step for the planner to update, and T_p is the planner step. The usage of v_{start} and a_{start} will be introduced shortly.

C. Longitudinal low-level controllers

As shown in Fig.1, for each step in the low-level loop, the processor *LongControl* adopts the most recent upper-level planning variables (v_{target} or a_{target} , v_{start} and a_{start}) updated at 20hz and calculates setpoints v_{pid} or a_{pid} for each low-level iteration running at 100 hz. Simultaneously the PI or PIF uses v_{pid} or a_{pid} to output the *control* variable and feeds it to gas/brake system. For the low-level control loop, it is important to understand how *LongControl* calculates v_{pid} or a_{pid} . The detailed algorithm is introduced as follows.

If the planner gives a target speed v_{target} , the low-level controller is usually a PI controller. Let \hat{t} denote the planning time where the sensor and planner get updated every 0.05s, and t is the low-level control time with step of 0.01. The algorithm to compute v_{pid} can be found in Openpilot 0.3.5 and the pseudo-code is shown in Algorithm 1 below.

In short, the current $v_{pid}(t)$ in a PI controller updates itself by moving towards the given $v_{target}(\hat{t})$ at a maximum rate bounded by some constraints including the acceleration limits.

If the upper-planner outputs the desired acceleration a_{target} , then the low-level control loop usually outputs the acceleration setpoint a_{pid} as well as v_{pid} . A feedforward term $k_f \cdot a_{pid}$ is added to form a PIF controller. In Algorithm 2, we show the algorithm for computing a_{pid} and v_{pid} using the a_{target} , v_{start} and a_{start} from a MPC longitudinal planner. Recall the two surrogate variable v_{start} and a_{start} are updated in the MPC planning loop.

Then we introduce how PI/PIF calculate the *control* input. Define the true speed as v_{ego} at each control time t , the speed error as $e = v_{pid} - v_{ego}$, the formulation of PI/PIF *control* input is expressed as:

Algorithm 1 Algorithm for v_{pid} with a linear planner

Input: v_{target} , $v_{pid}(t)$, $v_{ego}(t)$, a_{max} and a_{min}
Output: $v_{pid}(t+1)$

Initialisation: $v_{pid}(0) = v_{ego}(0)$
constant: overshoot allowance $oa = 2.0$
Start loop to compute $v_{pid}(t)$ for $t \in [\hat{t}, \hat{t} + 1]$:
1: **if** $v_{pid} > v_{ego} + oa$ and $v_{target} < v_{pid}$ **then**
2: $v_{pid} \leftarrow \max(v_{target}, v_{ego} + oa)$
3: **else if** $v_{pid} < v_{ego} - oa$ and $v_{target} > v_{pid}$ **then**
4: $v_{pid} \leftarrow \min(v_{target}, v_{ego} - oa)$
5: **end if**
6: **if** $v_{target} > v_{pid} + a_{max} \cdot dt$ **then**
7: $v_{pid} \leftarrow v_{pid} + a_{max} \cdot dt$
8: **else if** $v_{target} < v_{pid} + a_{min} \cdot dt$ **then**
9: $v_{pid} \leftarrow v_{pid} + a_{min} \cdot dt$
10: **else**
11: $v_{pid} \leftarrow v_{target}$
12: **end if**

Algorithm 2 Algorithm for a_{pid} , v_{pid} with an MPC planner

Input: most recent a_{target} , a_{start} , v_{start}

Output: a_{pid} and v_{pid}

Reset: $v_{start}(0) = v_{ego}(0)$ and $a_{start}(0) = a_{ego}(0)$
Low-level loop for $v_{pid}(t)$, $a_{pid}(t)$ for $t \in \{\hat{t}, \hat{t} + 0.01 \dots \hat{t} + d\hat{t}\}$:
1: $dt = t - \hat{t}$
2: $a_{pid}(t) = a_{start} + dt(a_{target} - a_{start})/dt_p$
3: $v_{pid}(t) = v_{start} + dt(a_{pid}(t) + a_{start})/2$

$$control = k_p \cdot e + k_i \cdot \int_0^t e(\tau) d\tau + k_f \cdot a_{pid} \quad (9)$$

where k_f , k_i and k_p correspond to the control gain for proportional(P), integral(I) and feedforward(F) terms. Note that they can all be constants or speed-dependent parameters.

The *compute_gb* function then views the *control* input as a desired acceleration and maps it to the desired gas/brake percentage *gb*:

$$gb = compute_gb(control, v_{ego}) \quad (10)$$

Note that brake is negative, and *gb* ranges from [-1,1]. The gas/brake commands are sent to the control interface of the car, where the dynamics between the *gb* and the produced acceleration can be represented as the *gb2accel* function:

$$a_{ego} = gb2accel(gb) \quad (11)$$

We will later show for real cars the *gb2accel* can be well approximated by a simple scaling function, for example, $a_{ego} = 3gb$, and accordingly the *compute_gb* function should share the same scale factor in the denominator, e.g. $gb = a_{ego}/3$. This can be achieved with the help of ACC module on recent car models. Advanced ACC control interfaces can accept scaled accelerations, or *gb* equivalently, as the input

and execute it using some unknown model. For these type of cars, one can view the gb as a scaled acceleration. We consider $gb2accel$ and $compute_gb$ functions are 'perfect' if they just use a single scale factor and match each other.

III. METHODOLOGY

This section investigates the impact of low-level controllers through analytical derivation. Correspondingly, we study the two types of controllers corresponding to linear/MPC planners.

Assuming the $compute_gb$ and $gb2accel$ functions are "perfect" (i.e., the desired acceleration requested by the $control$ will approximately equal to the true acceleration a_{ego} responses from the car), we have:

$$a_{ego} \approx control = k_p \cdot e + k_i \cdot \int_0^t e(\tau) d\tau + k_f \cdot a_{pid} \quad (12)$$

Then the whole control loop can be explicitly modeled and we can study the underlying interactions between low-level controller and the planner.

A. PI low-level controller and its impact on SS

Consider that the proportional gain has a dominant effect, and in discrete-time implementation the integral gain and derivative gain can all be converted into proportional gain, we omit the integral and derivative term for now:

$$a_{ego} = control \approx k_p(v_{pid} - v_{ego}) \quad (13)$$

For a linear planner as (1) and (2), it satisfies:

$$\begin{aligned} s_{lead} &= v_{lead} - v_{ego} = v_{rel} \\ s_{des} &= H_t v_{lead} \\ v_{lead} &= a_{lead} \end{aligned} \quad (14)$$

Substituting (14) into (2), we have:

$$v_{target} = k_v(v_{lead} - v_{ego}) + (1 - k_v H_t) a_{lead} \quad (15)$$

To investigate the impact on SS, we evaluate the maximum changes in the ego vehicle target speed, namely Δv_{target} , which can be calculated by tracking (15) from the time T_1 when the ego car starts to react to the lead vehicle, to the time $T_1 + \Delta T$ when the ego car starts to reduce the overshoot/undershoot (see Fig.2(e)):

$$\begin{aligned} \Delta v_{target} &= v_{target}(T_1 + \Delta T) - v_{target}(T_1) \\ &= \sum_{T_1 \leq \hat{t} \leq T_1 + \Delta T} k_v(v_{lead}(\hat{t}) - v_{ego}(\hat{t})) dt \\ &+ \sum_{T_1 \leq \hat{t} \leq T_1 + \Delta T} (1 - k_v H_t) a_{lead}(\hat{t}) dt \\ &= k_v \sum_{T_1 \leq \hat{t} \leq T_1 + \Delta T} v_{rel}(\hat{t}) + (1 - k_v H_t) \bar{a}_{lead} \Delta T \end{aligned} \quad (16)$$

where \bar{a}_{lead} is the average acceleration for the lead vehicle during ΔT . Since v_{lead} and a_{lead} do not change with the follower, the magnitude of the speed change for the ego vehicle will only depend on v_{rel} . Also note that $1 - k_v H_t > 0$ for rational values.

Then we subtract the lead vehicle speed change during ΔT , to yield the SS index of linear planner I_{linear} :

$$\begin{aligned} I_{linear} &= (|\Delta v_{target}| - |\Delta v_{lead}|) / |\Delta v_{lead}| \\ &= \frac{k_v}{|\Delta v_{lead}|} \left(\sum_{T_1 \leq \hat{t} \leq T_1 + \Delta T} |v_{rel}(\hat{t})| - H_t |\bar{a}_{lead}| \Delta T \right) \end{aligned} \quad (17)$$

which can be applied to both acceleration and deceleration cases. A smaller I_{linear} is desirable as it corresponds to better SS. If $I_{linear} > 0$ the speed change is amplified from leader to the follower, yielding a string unstable case. Although (17) does not directly involve low-level variables, the impact of the low-level controller can be described as: for a fixed planner, a slow-response controller moves the follower more slowly, which further makes the relative speed v_{rel} larger, and also takes longer ΔT to stabilize. A faster controller can track the planned speed faster, reduces the speed amplification Δv_{target} and thus improves SS.

The SS index (17) also sheds some light to the impact of the planner. Note that k_v , i.e., how fast the planner react to spacing, and the desired headway H_t can affect SS as well. If the planner is more sensitive to spacing change (i.e., with a larger k_v), the ACC system is more likely to be string unstable (i.e., larger Δv_{target} will make the planned trajectory harder to track). For the impact of time headway H_t , (17) indicates larger headway can benefit the SS, which is consistent with the recent empirical finding [20] from a few commercial ACC systems. Remarkably, the theoretic analysis of string stability in frequency domain also achieves the similar finding but in a different way, i.e. the larger time headway can reduce the ∞ -norm and 2-norm of the string stability transfer function [10], [17], [21].

B. PIF low-level controller and its impact on SS

As stated before, a PIF controller works with an MPC planner. Recall Algorithm 2 uses a_{target} , v_{start} and a_{start} to calculate the low-level setpoints $vPid$ and $aPid$.

In (8), we can assume the initial a_{start} equals to zero, thus the a_{start} sequence can be simplified using only a_{target} from the MPC planner, which leads to:

$$a_{start}(\hat{t}) = \sum_{n=0}^{\lfloor \hat{t}/d\hat{t} \rfloor - 1} \frac{d\hat{t}}{dt_p} (1 - d\hat{t}/dt_p)^{\lfloor \hat{t}/d\hat{t} \rfloor - 1 - n} a_{target}(nd\hat{t}) \quad (18)$$

where $\lfloor \hat{t}/d\hat{t} \rfloor$ is a floor function to calculate index for planning step of \hat{t} starting from zero. Substitute (18) into (8), the changes of v_{start} can be described using a_{target} :

$$\begin{aligned} 2/d\hat{t} \cdot \Delta v_{start} &= \sum_{T_1 \leq \hat{t} \leq T_1 + \Delta T} a_{target}(\hat{t}) + \\ &\sum_{n=0}^{\lfloor \hat{t}/d\hat{t} \rfloor} d\hat{t}/dt_p (1 - d\hat{t}/dt_p)^{\lfloor \hat{t}/d\hat{t} \rfloor - 1 - n} a_{target}(nd\hat{t}) \end{aligned} \quad (19)$$

Correspondingly, the SS index of MPC planner I_{mpc} given a MPC planner can be derived as:

$$\begin{aligned}
 I_{mpc} &= (|\Delta v_{start}| - |\Delta v_{lead}|) / |\Delta v_{lead}| \\
 &= -1 + \sum_{T_1 \leq \hat{t} \leq T_1 + \Delta T} |a_{target}(\hat{t})| \frac{d\hat{t}}{2|\Delta v_{lead}|} \\
 &\quad + \sum_{n=0}^{\lfloor \hat{t}/d\hat{t} \rfloor} \frac{d\hat{t}(1 - d\hat{t}/dt_p)^{\lfloor \hat{t}/d\hat{t} \rfloor - 1 - n}}{dt_p |\Delta v_{lead}|} |a_{target}(n d\hat{t})| \quad (20)
 \end{aligned}$$

Similarly, smaller I_{mpc} means better SS. Here for an MPC controller, a slow low-level controller will trigger the planner to produce larger desired acceleration $|a_{target}(nd\hat{t})|$ and thus increase the I_{mpc} , which means the SS is undermined.

In this section we tried to derive two indexes to measure the SS for the linear+PI and the MPC+PIF ACC systems. The mathematical derivations in (17) and (20) do not have explicit low-level variables yet, but they suggest the same finding that a fast controller (which enables faster decay of tracking error) can help the SS and vice versa. Note that (17) and (20) also indicate the SS is resulted from the interactions and coupling effect between the planner and the low-level controller. Attentive readers may already notice that our indexes are essentially the same the well-known transfer function used in control theory, but they are derived in time domain, not the frequency domain. A strict proof is omitted due to the page limit.

IV. SIMULATION RESULTS

This section justifies the theoretic findings through simulations, running on the same planner and low-level control algorithms. To simulate the actuator system, we assume $gb = \frac{1}{3}control$ and $a_{ego} = 3gb$. The assumption will be justified by data from real cars in the following section.

A. Actuator performance

First we investigate the impact of gas/brake system (the $gb2accel$ function). While the $compute_gb$ implies $gb = \frac{1}{3}control$, the true acceleration induced by the gb values are unknown, which could be larger or smaller than $control$. The unknown relationship from gas/brake to true acceleration is largely depending on each vehicle's engine and braking performance. Although the dynamics might be complex, we can define whether the actuator is overshooting if $a_{ego} > control$, or undershooting if $a_{ego} < control$. Now we present the impact of an undershooting actuator and an overshooting actuator on SS of a linear+PI ACC system. The simulation results are shown in Fig.2 and Fig.3, respectively.

As comparison, the overshooting actuator; see Fig.3(e); achieves significantly better SS than the undershooting actuator; see Fig.2(e). As for the tracking error, we see the slow controller has larger error indicated by the P term which is proportional to the speed error; see Fig.2(d) and Fig.3(d). Also, for the time ΔT that the follower needs to stabilize, Fig.2(e) and Fig.3 suggest the slow controller needs longer time. Both findings are consistent with our interpretation of the mathematical derivations (17) and (20).

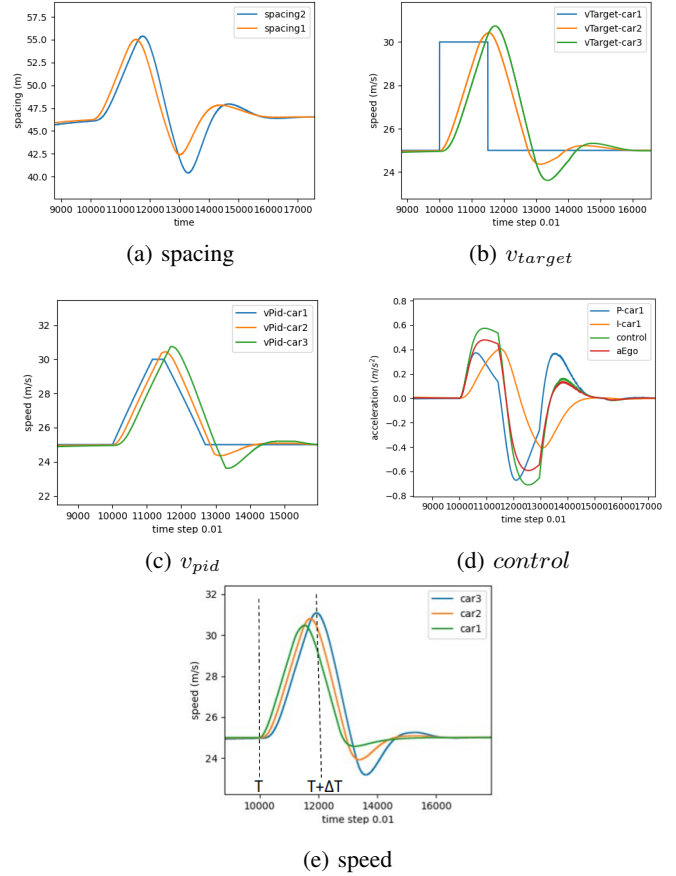


Fig. 2: The impact of an undershooting actuator on SS: the order of the figures are intended to show the cause and effect but it is a loop indeed.

B. Control gains

Now we investigate the impact of the control gains, and assume the actuator system is not undershooting or overshooting. In simulation, it means $gb = control/scale$ and $a_{ego} = scale * gb$ share the same $scale$ parameter. This assumption will be verified with data from real cars.

1) *Integral gain:* While integral (I) gain is designed to reduce steady-state error and is almost indispensable in real-world implementation, it also brings negative effect known as the integral windup. For longitudinal control of vehicles, we notice I gain can: i) sometimes have opposite sign against the proportional term (see Fig.4(c)), which further cancels out the proportional control for reducing the error; ii) accumulate quickly with a rapid speed changes in target speed, which can undermine SS; and iii) take long time to settle down. Accordingly, inappropriate I gain can make the controller slower and cause frequent overshoot from the setpoint, as shown in Fig.4(b). Combining the two effects, we see a string unstable platoon in Fig.4(a).

2) *Proportional gain:* For a controller with only proportional (P) gain, the impact of P gain is similar to the actuator's overshooting or undershooting effects, given the perfect

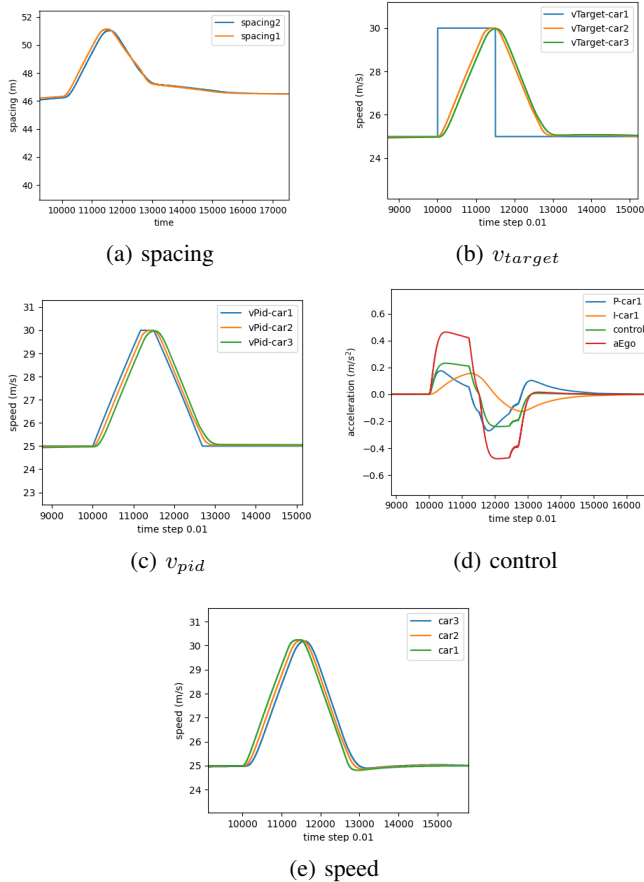


Fig. 3: The impact of an overshooting actuator on SS

compute_gb function and the *gb2accel* introduced in section II. From Fig.4(d), we can see a scaled P gain changes the *control* in the same way that a scaled *gb2accel* function does. Thus, it is safe to say increasing P gain could help SS as an overshooting actuator does. Due to the space constraints, we briefly show the differences of SS from low-level controllers with small P gain and with large P gain.

3) *Feedforward gain*: In a PIF controller, the feedforward term is $K_f \cdot a_{pid}$. Overall P works to reduce speed error and feedforward (F) gain is directly giving acceleration command, thus F gain is usually set as 1 and dominates the control input among the three gains in PIF controller. In simulation we run the MPC+PIF loop and conducted a comparison between a default and doubled F gain, as shown in Fig.6.

The comparison results suggest that tuning up the F gain can also make the low-level controller faster, see Fig.6(b) and (d), which improves the SS; see Fig.6 (a) and (c). We also observed that P and I terms can sometimes be contrary to the F term because a_{pid} and $e = v_{pid} - v_{ego}$ can have different signs. Notice that although $2K_f$ brings better SS, the controller is over fast since it creates oscillations in steady state. Thus, a proper F gain for preventing over-sensitive to small errors is also necessary.

To sum up, for the impact of control gains on the SS, we

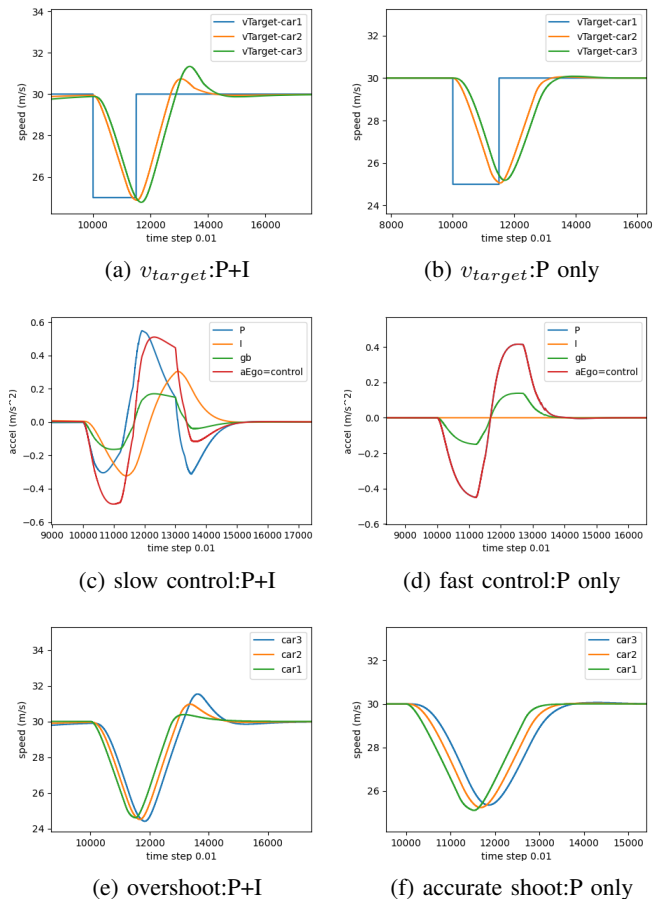


Fig. 4: The impact of integral term on SS

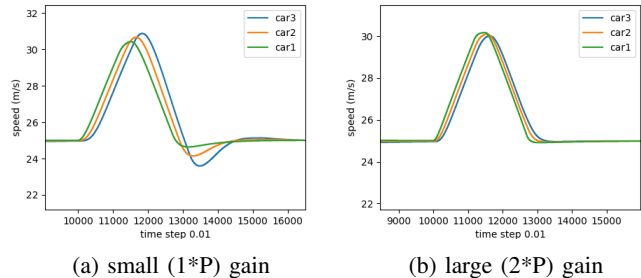


Fig. 5: Impact of P gain on SS

verify the similar conclusion for either the P or F gain with respect to PI/PIF controller. Also we displayed the negative impact of integral windup.

V. VALIDATION ON REAL CARS

In this section we validate the above findings using data from commercial vehicles running the ACC algorithms. Specifically, we use Comma Two, an after-market device from Comma.ai that can overwrite the stock ACC commands. The

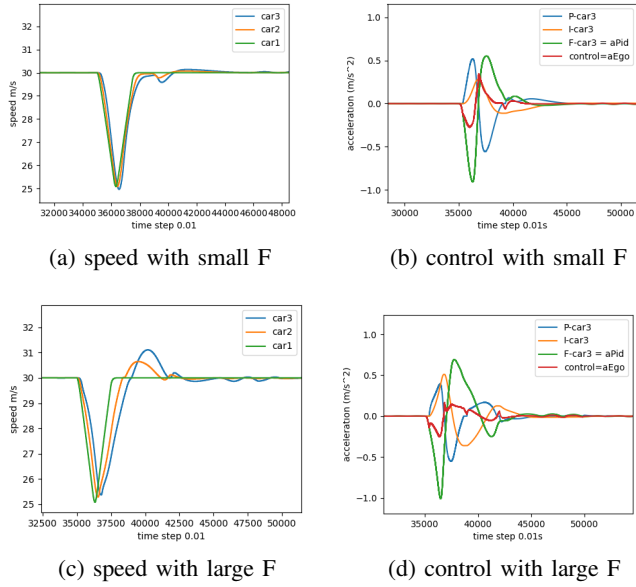


Fig. 6: The impact of F gain on SS

authors have a custom fork¹ of the Openpilot and have published some branches with the different upper-level planners and low-level controllers mentioned before.

A. Relation between gas/brake to acceleration

First we show the data collected from a 2020 Toyota Corolla and a 2019 Honda Civic, as validation for the assumption of a "perfect" *compute_gb* function we used in simulations.

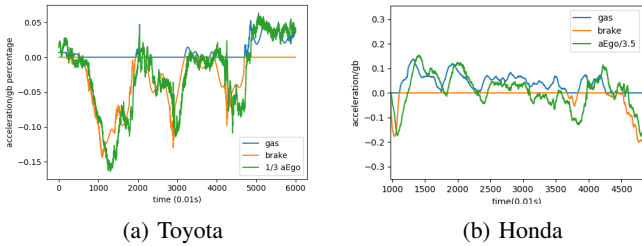


Fig. 7: Relation between gas/brake and acceleration on real cars

Fig.7 proves that a simple scale function is a good fit to the relationship between gas/brake and true acceleration. Note that we are using market vehicles without any modifications on the hardware system. This means the relationship can be easily transferred.²

¹<https://github.com/HaoZhouGT/openpilot>: Includes implementation of ACC+PI, MPC+PIF, and IDM+PIF for self-driving longitudinal control

²This finding is a bit surprising but may be explained by the modern ACC modules that can accept direct acceleration commands as inputs and execute the acceleration in a desired manner. However, indeed we are not sure the *gb* is gas/brake percentage, they might be very likely a scaled desired acceleration that ACC modules will execute. According to Openpilot community [22], at least the new ACC modules from General Motor and Toyota after 2020 are potentially using such a logic.

B. Validation of the impact of integral windup

Integral windup can induce overshooting from a low-level controller to the overshooting of lead vehicle speed and thus undermines the SS. The Fig.8(a) showcases a string unstable example where the follower overshoots the lead vehicle around step 3500, meanwhile the Fig.8(b) clearly shows that integral windup (orange curve) is happening and dominates the control.

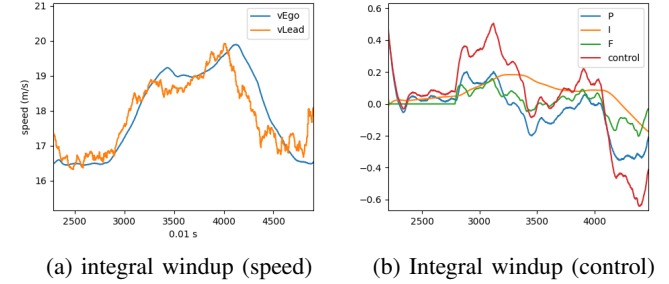


Fig. 8: Impact of integral on SS in a real drive

C. Validation of the impact of a fast/slow low-level controller

As indicated before, the P or F gains and the gas/brake system share the similar mechanism to affect the SS by making the low-level controller faster or slower. The major finding is that a fast low-level controller improves SS and the slower controller undermines it.

To verify this, we compare two low-level controllers sharing the same planner (MPC) but with different low-level parameters. Specifically, the fast low-level controller uses $1.0K_p$, $0.33K_i$, $1.2K_f$ and an overshooting *compute_gb* defined as $gb = 1/3 \cdot control$. By contrast, the slow low-level controller adopts $0.5K_p$, $0.33K_i$, $1.0K_f$ and an undershooting *compute_gb* defined as $gb = 1/5 \cdot control$. The numbers before control gains are scales of the default values.

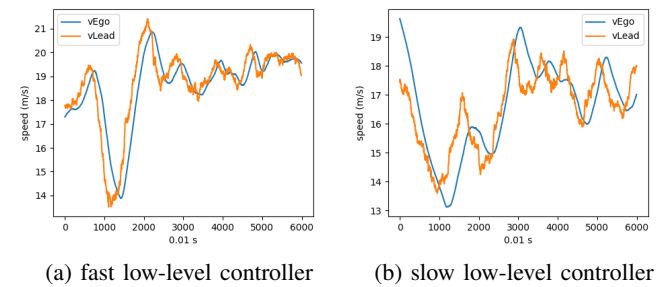


Fig. 9: Impact of a fast/slow low-level controller on SS

Fig.9 displays the two real-world drives using a fast/slow low-level controller. The ego vehicle follows a human-driven lead vehicle in natural driving where the lead vehicle changes its speed occasionally on a curvy road. It is apparent that the fast low-level controller is able to dampen the lead speed changes while the slow low-level controller amplifies them. The results suggests better SS can be obtained from a fast low-level controller.

To show how a fast low-level controller achieve SS, Fig.10 (a) displays the detailed P, I, F terms in the *control* input. As stated before, a more dominating F term can help SS, and P gain is expected to be consistent with F term, not canceling out its effect. Also we would like to limit the impact of integral windup. Additionally, Fig.10(b) shows that v_{start} is close to v_{ego} , which supports our method to use v_{start} to investigate the impact on SS in III.

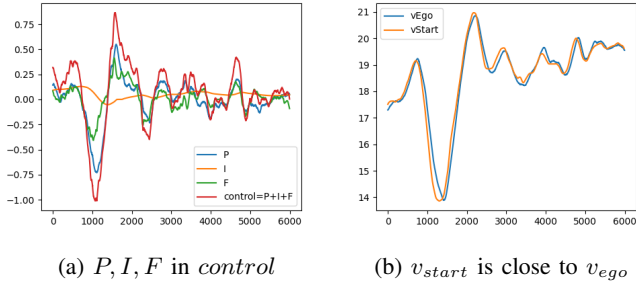


Fig. 10: A real SS ACC with a fast low-level controller

VI. CONCLUDING COMMENTS AND OUTLOOK

The paper introduces, for the first time, the open-source factory ACC algorithms to literature and studies the impact of low-level controller on SS. In a nutshell, the study finds a fast-response low-level controller can improve SS while a slow-response controller can undermine it despite of a string stable planner. Accordingly, we suggest putting more efforts on improving the low-level controller rather than designing more string stable ACC/CACC models which are already available for modern cars.

We suggest future directions on: i) anti-windup design for the integral term in low-level control; ii) special treatment for grade/curve to improve SS and iii) quantifying the potential "conflict" between a fast low-level controller and comfortable-ness or safety.

ACKNOWLEDGMENT

The authors would like to acknowledge the warm help from Joe Pancotti for his commit in modifying the Honda Bosch interface [23]. We also appreciate the helpful discussions with Shane Smiskol and csouers at Openpilot's community.

REFERENCES

- [1] E. Shaw and J. K. Hedrick, "String stability analysis for heterogeneous vehicle strings," in *2007 American Control Conference*, 2007, pp. 3118–3125.
- [2] S. Feng, Y. Zhang, S. Li, Z. Cao, H. Liu, and L. Li, "String stability for vehicular platoon control: Definitions and analysis methods," *Annu. Rev. Control.*, vol. 47, pp. 81–97, 2019.
- [3] G. J. L. Naus, R. P. A. Vugts, J. Ploeg, M. J. G. van de Molengraft, and M. Steinbuch, "String-stable cacc design and experimental validation: A frequency-domain approach," *IEEE Transactions on Vehicular Technology*, vol. 59, no. 9, pp. 4268–4279, 2010.
- [4] J. Zhou and H. Peng, "Range policy of adaptive cruise control vehicles for improved flow stability and string stability," *IEEE Transactions on intelligent transportation systems*, vol. 6, no. 2, pp. 229–237, 2005.

- [5] G. Gunter, C. Janssen, W. Barbour, R. E. Stern, and D. B. Work, "Model-based string stability of adaptive cruise control systems using field data," *IEEE Transactions on Intelligent Vehicles*, vol. 5, no. 1, pp. 90–99, 2019.
- [6] M. Makridis, K. Mattas, B. Ciuffo, F. Re, A. Kriston, F. Minarini, and G. Rognelund, "Empirical study on the properties of adaptive cruise control systems and their impact on traffic flow and string stability," *Transportation research record*, vol. 2674, no. 4, pp. 471–484, 2020.
- [7] D. Yanakiev and I. Kanellakopoulos, "Variable time headway for string stability of automated heavy-duty vehicles," in *Proceedings of 1995 34th IEEE Conference on Decision and Control*, vol. 4. IEEE, 1995, pp. 4077–4081.
- [8] C.-Y. Liang and H. Peng, "Optimal adaptive cruise control with guaranteed string stability," *Vehicle system dynamics*, vol. 32, no. 4-5, pp. 313–330, 1999.
- [9] C. Liang and H. Peng, "String stability analysis of adaptive cruise controlled vehicles," *Isme International Journal Series C-mechanical Systems Machine Elements and Manufacturing*, vol. 43, pp. 671–677, 2000.
- [10] G. J. Naus, R. P. Vugts, J. Ploeg, M. J. van De Molengraft, and M. Steinbuch, "String-stable cacc design and experimental validation: A frequency-domain approach," *IEEE Transactions on vehicular technology*, vol. 59, no. 9, pp. 4268–4279, 2010.
- [11] V. Milanés, S. E. Shladover, J. Spring, C. Nowakowski, H. Kawazoe, and M. Nakamura, "Cooperative adaptive cruise control in real traffic situations," *IEEE Transactions on intelligent transportation systems*, vol. 15, no. 1, pp. 296–305, 2013.
- [12] G. Gunter, D. Gloudemans, R. E. Stern, S. McQuade, R. Bhadani, M. Bunting, M. L. Delle Monache, R. Lysecky, B. Seibold, J. Sprinkle *et al.*, "Are commercially implemented adaptive cruise control systems string stable?" *IEEE Transactions on Intelligent Transportation Systems*, 2020.
- [13] V. Milanés and S. E. Shladover, "Modeling cooperative and autonomous adaptive cruise control dynamic responses using experimental data," *Transportation Research Part C: Emerging Technologies*, vol. 48, pp. 285–300, 2014.
- [14] comma.ai. comma.ai – introducing openpilot. [Online]. Available: <https://comma.ai/>
- [15] Y. Zhou and S. Ahn, "Robust local and string stability for a decentralized car following control strategy for connected automated vehicles," *Transportation Research Part B: Methodological*, vol. 125, pp. 175–196, 2019.
- [16] M. Diehl, "Toolkit for automatic control and dynamic optimization." [Online]. Available: <https://acado.github.io/>
- [17] S. Gong, A. Zhou, and S. Peeta, "Cooperative adaptive cruise control for a platoon of connected and autonomous vehicles considering dynamic information flow topology," *Transportation Research Record*, vol. 2673, no. 10, pp. 185–198, 2019.
- [18] H. Zhou, "Details of the mpc for longitudinal control without a neural network." [Online]. Available: <https://howardchow92.medium.com/details-of-the-mpc-for-longitudinal-control-without-a-neural-network-f255abd1c2ed>
- [19] —, "The MPC designed for end-to-end longitudinal self-driving at OpenPilot, Comma.ai." 2020. [Online]. Available: <https://howardchow92.medium.com/the-model-mpc-designed-for-end-to-end-longitudinal-self-driving-at-openpilot-comma>
- [20] T. Li, D. Chen, H. Zhou, J. Laval, and Y. Xie, "Car-following behavior characteristics of adaptive cruise control vehicles based on empirical experiments," *Transportation Research Part B: Methodological*, vol. 147, pp. 67–91, 2021.
- [21] S. Klinge and R. H. Middleton, "Time headway requirements for string stability of homogeneous linear unidirectionally connected systems," in *Proceedings of the 48th IEEE Conference on Decision and Control (CDC) held jointly with 2009 28th Chinese Control Conference*, 2009, pp. 1992–1997.
- [22] S. Smiskol, "Discussion on the "compute_gb" function in openpilot community," 2021.
- [23] J. Pancotti, "The git commit that makes honda bosch vehicle to have a vision-based openpilot control." [Online]. Available: <https://github.com/jpancotti/openpilot/commit/468b89a>